Journal of the Chinese Society of Mechanical Engineers, Vol.46, No.6, pp609~617 (2025)

Numerical Analysis and Experimental Verification of Oxygen Concentration in an Oxygen-Free Oven

Jhen-Syuan Huang*, Cian-Shun Luo** and Chi-Chang Wang***

Keywords： Oxygen-Free Oven, Mass Transfer, Numerical Analysis, Air Permeation.

ABSTRACT

This study investigates the transient variation of oxygen concentration in an oxygen-free oven using two numerical methodologies and experimental validation. A two-dimensional model, based on the finite element method, is developed to analyze velocity fields and oxygen concentration distributions, incorporating convection and diffusion effects. Additionally, a zero-dimensional model is introduced to simplify the prediction of oxygen concentration under convection-dominant conditions. The models are validated against experimental data obtained from a semiconductor processing oven in case of different nitrogen flow rates. The results indicate that both models effectively predict oxygen concentration reduction, with deviations from experimental values remaining within 3.3%. Furthermore, the influence of air permeation is examined, and its significant impact on oxygen concentration dynamics is revealed. These findings provide valuable insights for optimizing oxygen-free oven designs and improving process reliability in industrial applications.

INTRODUCTION

Heat treatment processes are crucial in various industries, ensuring material quality and manufacturing performance. Industrial ovens, such as vacuum annealing furnaces for semiconductor wafer production, multi-layer furnaces for glass panel processing, the printing industry, and the oxygen-free oven investigated in this study, are essential tools in these processes. Before heat treatment, nitrogen (N_2) is often injected into these ovens to create an environment of low oxygen concentration, preventing oxidation and other undesirable reactions in materials exposed to high temperatures. This step is crucial for maintaining the quality and yield of subsequent heat treatment processes. Nitrogen, which makes up approximately 78% of the Earth's atmosphere, is one of the most abundant elements in the air. It is colorless, odorless, and tasteless, making it highly suitable for diverse industrial applications, including semiconductor manufacturing, electronics, chemicals, aerospace, precision manufacturing, food processing, and medical industries. The presence of oxygen in heat treatment environments can influence reaction rates and affect the formation of products. As such, controlling oxygen concentration is critical for achieving precise processing.

To explore the performance of oxygen-free ovens, it is essential to understand their design and configurations by reviewing relevant studies. Verboven et al. (2000) used fundamental energy and momentum equations in fluid dynamics to describe airflow and temperature variations in industrial forced convection ovens. Their findings revealed that, in an empty oven, the flow field generated vortices concentrated on one side. However, placing polymer bricks reduced these vortices, promoting more horizontal airflow and better temperature uniformity. Ramirez-Labore et al. (2016) analyzed convection and radiation transfer in electric ovens during uniform food cooking. By establishing differential heat transfer equations, they effectively estimated heat flux and energy transfer within different regions of the oven, providing insights into the relationship between cooking time, energy consumption, and oven performance under varying conditions. Abraham and Sparrow (2004) developed algebraic equations based on the first law of thermodynamics to predict temperature variations of heat loads in ovens under radiation and convection conditions. Their study demonstrated that the predicted temperatures depended on the surface emissivity of the load, with good agreement observed between predictions and experimental data. Kokolj et al. (2017) utilized numerical simulations to solve the Navier-Stokes

Paper Received February, 2025. Revised April, 2025. Accepted April, 2025. Author for Correspondence: Jhen-Syuan Huang.

* *Assistant Professor, Department of Mechanical and Computer-Aided Engineering, Feng Chia University, Taichung City, Taiwan.*
** *Graduate Student, Department of Mechanical and Computer-Aided Engineering, Feng Chia University, Taichung City, Taiwan.*
*** *Professor, Department of Mechanical and Computer-Aided Engineering, Feng Chia University, Taichung City, Taiwan.*

equations based on temperature, convection speed, and other operating conditions in ovens. They modeled browning during baking processes and validated the model's predictive capabilities. The results showed that water vapor and its phase-change latent heat absorption significantly affected temperature and heat distribution in ovens and baked goods. Isleroglu and Kaymak-Ertekin (2016) developed a two-dimensional heat and mass transfer model for steam-assisted hybrid ovens. By solving coupled partial differential equations, they predicted the influence of moisture concentration on food during baking, including the diffusion coefficient and total steam content. The model exhibited excellent agreement with experimental data. Lucchi and Lorenzini (2019) employed numerical simulations based on fluid dynamics principles to analyze the transient behavior of the internal flow field in professional ovens under natural convection. Their results highlighted that the convective coefficient of the flow field was a critical factor affecting heating efficiency and temperature uniformity. Tudon-Martinez et al. (2019) proposed a zero-dimensional thermodynamic model for designing industrial furnaces based on the energy conservation. Considering convection and radiation efficiency, their analysis achieved 96.77% agreement with experimental data for total heat flux and temperature distribution. This simplified model required only 5% of the processing time compared to traditional complex two-dimensional models. Tan et al. (2013) simulated temperature distribution and thermal performance in different zones of large slab reheating furnaces. They developed two-dimensional and three-dimensional mathematical models based on energy balance and radiation equations, validated by industrial furnace measurements, with consistent results and no significant differences in predictive ability between the two models. Meinicke et al. (2018) conducted operational measurements on loop heat pipe (LHP) systems to obtain extensive parameter data, which were used to establish thermodynamic models. These models accurately predicted the thermal behavior of heat pipes under varying temperature and pressure conditions, emphasizing the impact of heat leakage on operational conditions.

In addition to studies on the heating efficiency and temperature uniformity of ovens, another critical research focus is creating and maintaining low-oxygen environments within ovens during the initiation and progression of baking processes. Maier et al. (2019)0 experimentally and analytically evaluated the effects of processing in oxygen-free and oxygen-rich environments. Using tungsten carbide tools for dry machining titanium-based alloys, they found that oxygen-free conditions effectively reduced surface oxidation and contamination, improving surface smoothness and precision. Zhang et al. (2018) investigated the propagation behavior of dust explosion flames in semi-enclosed explosion tubes. By employing monetization techniques to reduce oxygen concentration, they observed that lower oxygen levels significantly slowed flame propagation rates and altered flame morphology and stability. Similarly, Meng et al. (2019) studied the preparation of high-oxidation-resistant bonding coatings for thermal barrier coatings using MCrAlY alloys under low-oxygen heat treatment. Their experimental results revealed that reducing oxygen content minimized the growth of thermally grown oxide (TGO) layers, enhanced the oxidation resistance of the coatings, and prevented the exposure of metallic phases from alumina deposits on the coating surface. Strauß et al. (2019) examined the heating behavior of stainless steels AISI304 and AISI446 with natural oxide layers under high and ultra-high vacuum conditions. AISI446 exhibited stable phase behavior in both conditions, indicating that lower oxygen effectively inhibited the formation of new oxide layers. Pei et al. (2023)0 investigated the high-temperature oxygen-free treatment of polymer-modified asphalt, including styrene-butadiene-styrene (SBS) and chloroprene rubber (CR) high-viscosity asphalt. The results demonstrated that oxygen-free conditions during high-temperature treatment significantly reduced the viscosity of SBS and CR at operational temperatures, leading to improved durability and processing quality compared to air-exposed thermal curing. Lastly, Wegewitz et al. (2023) explored oxygen-free production processes, ranging from conceptual stages to practical applications in industries such as metal manufacturing, electronics production, and energy generation. They highlighted the addition of silane to inert gases, which facilitates the conversion of oxygen into silica, hydrogen, and water, allowing for the complete removal of oxygen. This approach had significantly reduced oxygen concentrations in industrial nitrogen streams.

Building on the aforementioned reviews and discussion, this study aims to establish predictive models for an oxygen-free oven by investigating nitrogen injection strategies to reduce oxygen concentration. A two-dimensional (2-D) model is first constructed and solved using the finite element method (FEM) to analyze the flow field and the convective and diffusive behavior of oxygen within the oven. The variations of the maximum, average, and minimum oxygen concentrations in the oven are further examined. To save computational cost, a zero-dimensional (0-D) model based on the principle of concentration diffusion is also put forward in this research. Additionally, as highlighted by Meinicke et al. (2018), the effect of unavoidable gas permeation is considered. Specifically, this study incorporates the permeation mass flow rate to account for diffusion-driven oxygen infiltration caused by pressure or concentration differences between the interior and exterior of the oven. The impact of this factor on oxygen concentration during the process is analyzed,

and the models' predictions are validated against experimental data to assess their accuracy and applicability.

EXPERIMENTAL EQUIPMENT AND SETUP

Fig. 1(a) shows the equipment used for validation in this study, an oxygen-free oven applied in semiconductor heat treatment processes. The oven is demonstrated with temperature variation within 1.5% at 300 °C and 2% at 500 °C. It is available in two cleanroom specifications, Class 10 and Class 100, making it superior in chip manufacturing. The quality of the finished product is significantly affected by the oxygen concentration inside the oven since wafers, electronic components, and packaging materials are prone to react with oxygen at high temperatures. As a result, pure nitrogen is usually introduced to replace the internal air and create an oxygen-free environment. Fig. 1(b) displays the structural composition of the oven, which comprises gas inlet and outlet ports, perforated plates, a circulation fan, an electric heating system, and high-efficiency particulate air (HEPA) filters. The operation can be acknowledged through the flow paths marked by red arrows in the figure. Pure nitrogen is injected through the inlet port, flows through the internal electric heating system, and then passes through the HEPA filter to remove particulates and impurities. Afterward, the gas flows through the perforated plate into the main working chamber and exits through the other perforated plate. A fan-driven system at the top recirculates the gas mixture, forming a loop to maintain the internal circulation. To stabilize the internal pressure, a portion of the mixed gas is discharged through the exhaust port at the bottom. The average oxygen concentration inside the oven is measured in real-time using an oxygen analyzer. The experimental data used in this study were provided by a local semiconductor equipment manufacturer. According to actual manufacturing parameters, measurements were carried out with nitrogen flow rates of 6.02×10^{-3}, 7.02×10^{-3}, and 8.02×10^{-3} (kg/s). The oxygen concentrations as a function of time serve as the basis for validating the predictive models developed in this study.

(a) Photo of the equipment.

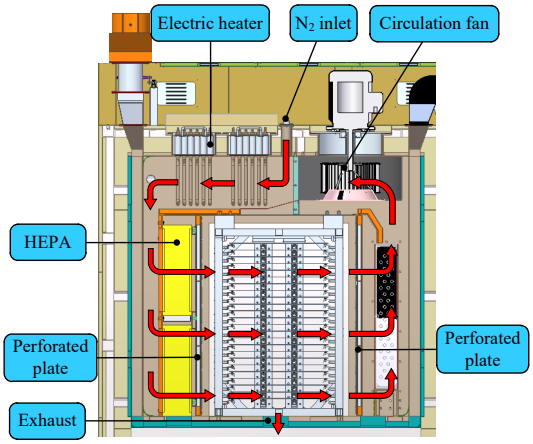

(b) Interior structure and components.

Fig. 1. Studied oxygen-free oven.

NUMERICAL ANALYSIS

Two-Dimensional Model

In this research, the above-mentioned oven is simplified with a two-dimensional geometry, where the flow domain is shown in Fig. 2. Structures such as the heating system, HEPA filters, fan assemblies, and support brackets are neglected to streamline the model. In the equipment, perforated plates for uniform distribution flow are fabricated by thin metal sheets with slots, and they are modeled as internal walls in the present simulation. The internal circulation fan is modeled by a volume force, which ensures that the volumetric flow rate within the oven meets the operational requirement. Pure nitrogen enters the inlet while the gas mixture expels the outlet. The flow is assumed to be laminar and incompressible. The present study focuses on the required time for decreasing the oxygen concentration to 100 ppm, in which the heat treatment process can be initiated.

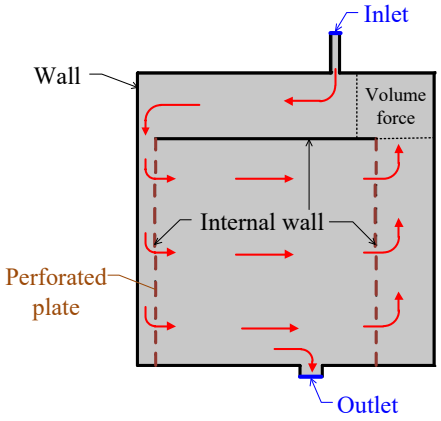

Fig. 2. Two-dimensional domain of the oxygen-free oven.

In two-dimensional analysis, the velocity and pressure fields within the oven are evaluated by continuity and the Navier-Stokes equation, and the oxygen concentration is computed based on the mass transfer equation. For incompressible flow, the continuity equation is written in

$$\nabla \cdot \vec{v} = 0, \tag{1}$$

The momentum equation can be expressed as

$$\rho\left(\frac{\partial \vec{v}}{\partial t} + \vec{v} \cdot \nabla \vec{v}\right) = -\nabla p + \mu \nabla^2 \vec{v} + \vec{F}, \tag{2}$$

where $\vec{F}$ is the volumetric force term, the gravity is ignored herein.

Mass transfer describing the concentration field is

$$\left(\frac{\partial C}{\partial t} + \vec{v} \cdot \nabla C\right) = D\nabla^2 C, \tag{3}$$

where C is the oxygen concentration. In this study, the above equations are numerically solved by the finite element method. For transient simulation, the initial conditions for velocity, pressure, and concentration are applied as

$$\vec{v}_0 = 0\ (m/s), \tag{4}$$

$$p_0 = 1.01325 \times 10^5\ (\text{Pa}), \tag{5}$$

$$C_0 = 2.1 \times 10^5\ (\text{ppm}), \tag{6}$$

As shown in Fig. 2, three kinds of boundary conditions, inlet, outlet, and wall (including internal wall), are applied in the FEM simulation. The boundary conditions are detailed as follows.

Inlet boundary conditions:

$$\vec{v} = -\frac{\dot{m}_{inN}+\dot{m}_{inP}}{\rho A_{in}}\vec{n}\ ,\ C = \frac{\dot{m}_{inP}}{\dot{m}_{inN}+\dot{m}_{inP}}C_P, \tag{7}$$

Outlet boundary conditions:

$$\frac{\partial \vec{v}}{\partial \tau} = 0\ ,\ \frac{\partial C}{\partial \tau} = 0\ ,\ p = 1.03325 \times 10^5\ (\text{Pa}), \tag{8}$$

Wall boundary conditions:

$$\vec{v} = 0\ ,\ \frac{\partial C}{\partial n} = 0\ ,\ \frac{\partial p}{\partial \tau} = 0, \tag{9}$$

where $\dot{m}_{inN}$ is the mass flow rate of nitrogen used to purge the oven. In this paper, air permeation due to pressure or concentration differences between the oven interior and exterior is considered. $\dot{m}_{inP}$ stands for the mass flow rate of air permeation, and C_P is the oxygen concentration of the permeated air (2.1×10^5 ppm). The leakage mechanisms often exhibit a behavior where the rate of gas permeation is influenced by the induced pressure differential caused by the nitrogen purging process (Bejan, 2013). A higher nitrogen flow rate creates a more significant positive pressure inside the chamber relative to the external atmosphere. This leads to a proportionally reduced infiltration rate due to the balance between convective and diffusive transport processes. Hence, it is assumed that air permeation is proportional to the purging nitrogen with a factor, λ, and they are related as

$$\dot{m}_{inP} = \lambda \dot{m}_{inN}, \tag{10}$$

This factor is incorporated at the inlet boundary to reflect the overall effects of sealing interfaces. The significance of air permeation will be discussed in detail in subsequent sections, along with its influence on oxygen concentration reduction.

Zero-Dimensional Model

Industrial ovens often incorporate high-speed fluid flow to reduce baking time and improve temperature uniformity. This characteristic results in convection effects dominating over diffusion in mixing gases inside the oven. Under such convection-dominant conditions, a zero-dimensional model, which assumes negligible spatial variations, becomes feasible. Based on the conservation of mass and concentration within a control volume, the governing equations can be expressed as:

$$\dot{m}_{out} = \dot{m}_{inN} + \dot{m}_{inP}, \tag{11}$$

$$\rho\forall\frac{d\bar{C}}{dt} = \dot{m}_{inP}C_P - \dot{m}_{out}\bar{C}, \tag{12}$$

The gas mixture inside the oven is considered incompressible, so the dependence of mass on time is ignored. $\bar{C}$ is the average volumetric oxygen concentration inside the oven and is only a function of time with zero-dimensional assumption. $\forall$ is the total volume of the oven. Since the oxygen concentration of the nitrogen inflow is zero, it has no contribution in Eq. (12). By combining the above two equations, an analytical solution of the transient concentration can be obtained:

$$\bar{C}(t) = \frac{\dot{m}_{inP}}{\dot{m}_{inN}+\dot{m}_{inP}}C_P + \left(C_0 - \frac{\dot{m}_{inP}}{\dot{m}_{inN}+\dot{m}_{inP}}C_P\right)e^{-\frac{\dot{m}_{inN}+\dot{m}_{inP}}{\rho\forall}t}, \tag{13}$$

This 0-D model provides a simplified yet effective framework for predicting the transient oxygen concentration inside the oven under convection-dominant conditions, making it highly applicable to industrial scenarios. In this paper, 2-D and 0-D simulations are proposed to evaluate the variation of

Table 1. Thermophysical and operational parameters used in the baseline case.

Parameter	Value
ρ	$1.204\ (\mathrm{kg/m^3})$
μ	$1.81 \times 10^{-5}\ (\mathrm{Pa \cdot s})$
D	$2.1 \times 10^{-9}\ (\mathrm{m^2/s})$
$\forall$	$1.39\ (\mathrm{m^3})$
$\dot{m}_{inN}$	$6.02 \times 10^{-3}\ (\mathrm{kg/s})$
$\vec{F}$	$-100\,\vec{\imath}\ (\mathrm{N/m^3})$
λ	10^{-5}

oxygen concentration in the oven. The thermophysical and operational parameters adopted in the numerical analysis are listed in Table 1. At a standard condition, gas constants of nitrogen and air are 296.8 J/kg·K and 287.1 J/kg·K, resulting in a 3.5% difference. Furthermore, their densities are 1.176 kg/m^3 and 1.204 kg/m^3, respectively. The relative density difference is then evaluated to be 2.3 %, and hence, constant density is taken throughout the analysis.

RESULTS AND DISCUSSION

Grid Verification

This study investigates the temporal variation of oxygen concentration in an oxygen-free oven with both simulations and experimental validation. A 2-D transient model is first performed by the FEM method to analyze the velocity field and further examine the convective effect of oxygen concentration. As depicted in Fig. 3, the triangular mesh is selected, and 2,293 elements are generated in the computational domain.

For the FEM simulation, the model requires preliminary mesh size testing to ensure accuracy. The comparison of average oxygen concentration across different elements is shown in Fig. 4. Element numbers of 1,193, 2,293, and 4,571 are tested in the present case. Significant discrepancy is observed between the results of 1,193 and 2,293 elements, while the results of 2,293 and 4,571 elements are closely aligned. It is found that beyond a mesh resolution of 2,293 elements, further refinement results in less than a 0.5% difference in oxygen concentration predictions while significantly increasing computation time. This validates the chosen mesh resolution as a balance between accuracy and efficiency. Therefore, a mesh size of 2,293 elements is deemed sufficient to ensure stable and accurate simulation results.

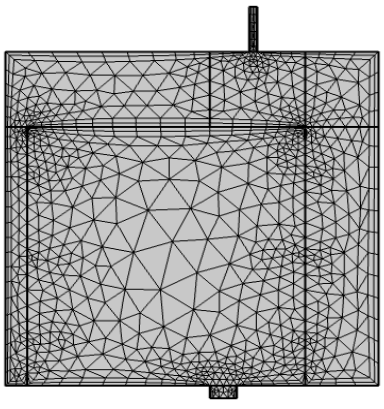

Fig. 3. Computational domain with 2,293 elements.

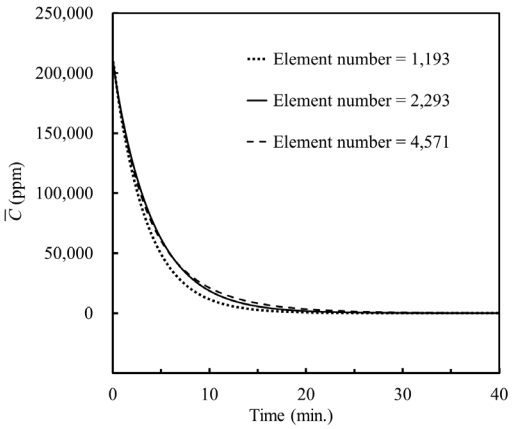

Fig 4. Comparison of average oxygen concentration over time under different element numbers.

Two-Dimensional Simulation

Fig. 5 illustrates the oxygen concentration distributions and flow streamlines at the 20, 40, 60, and 80 minutes by 2-D simulation. The concentration contours indicate the oxygen fraction, while the streamlines depicted by black lines and arrows represent the flow direction of the gas mixture. As shown in Fig. 5(a), the nitrogen from the top inlet mixes with the internal air, reducing the oxygen concentration. The fan-driven flow (a volume force) directs the gas through the chamber's perforated plates on the left and right sides, creating a vortex inside the chamber. Portions of the mixed gas with higher oxygen concentrations are expelled through the exhaust port at the bottom. As nitrogen is injected and mixed gas exits, the convection and diffusion effects gradually reduce the overall oxygen concentration in the oven and achieve a uniform low-oxygen environment over time, as shown in Fig. 5(b) and (c). Finally, a concentration of about 2 ppm is reached at the 80 minutes. A closer examination of Fig. 5 reveals the formation of a distinct closed vortex in the upper-left corner of the cavity at all time intervals. This vortex creates a region of circular flow that inhibits the convection-driven movement of gas toward the exhaust port, leaving diffusion as the primary mechanism for oxygen transport out of the vortex.

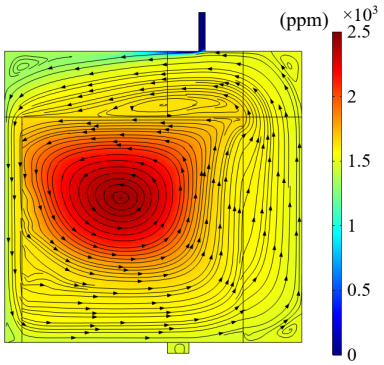

(a) 20 (min.)

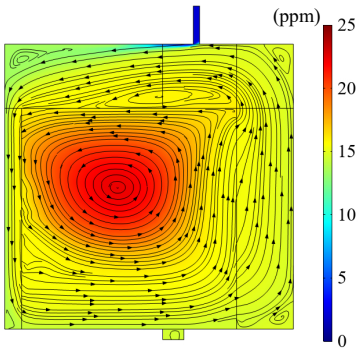

(b) 40 (min.)

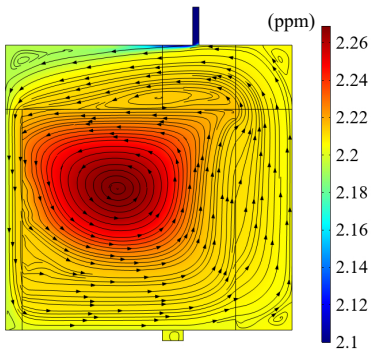

(c) 60 (min.)

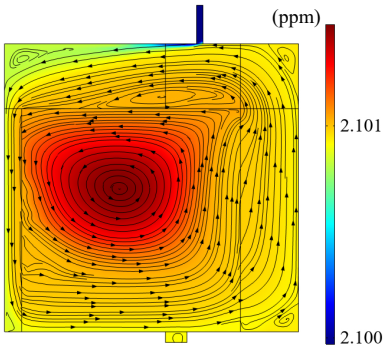

(d) 80 (min.)

Fig. 5. Concentration distribution and streamlines of mixed gas in the oven at different times.

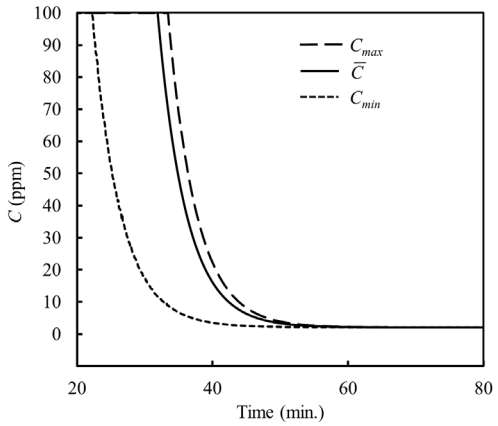

Fig. 6. Maximum, average, and minimum oxygen concentration curves of 2-D model.

Fig. 6 presents the temporal variations in the maximum, average, and minimum oxygen concentrations from the 2-D model as the values drop below 100 ppm, providing further insight into these dynamics. Due to the closed vortex, the rate of decline slows as time progresses, as diffusion becomes the dominant mechanism. The minimum oxygen concentration, occurring near the nitrogen inlet, shows a significant difference compared to the average and maximum concentrations, suggesting that the average and maximum concentrations are better indicators of the overall oxygen distribution in the oven.

Effect of Permeation Factor

There is always some degree of leakage or gas permeation in industrial applications, whether in oxygen-free, pressurized, or vacuum-heating furnaces. These effects are primarily due to pressure differentials or differences in oxygen concentration between the interior and exterior of the oven. In this study, a permeation factor is proposed to include air permeation and is used in both 2-D and 0-D models. Fig. 7 compares the experimental results of average oxygen concentration with different values of permeation factors applied in the 2-D and 0-D models, respectively. It can be found from Fig. 7 (a) and (b) that a factor of 10^{-4} deviates from the experiment and stagnates around 20 ppm ultimately. The simulation results align more closely with experimental trends as the factor is adjusted to 10^{-5} and 10^{-6}. However, the key difference between 10^{-5} and 10^{-6} lies in the degree of agreement with experimental data. For $\lambda = 10^{-5}$, the oxygen concentration reduction trend closely matches experimental observations, resulting in better consistency with experimental data. This analysis underscores the significant influence of air permeation on oxygen concentration dynamics and highlights the importance of considering the permeation effect when modeling and validating oxygen-free ovens. To address sensitivity of permeation factor, simulations are conducted over an extended range: $\lambda = 10^{-4}$ (higher

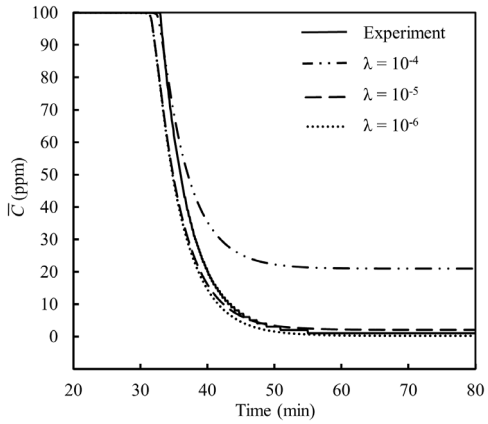

(a) Comparison between experiment and 2-D model.

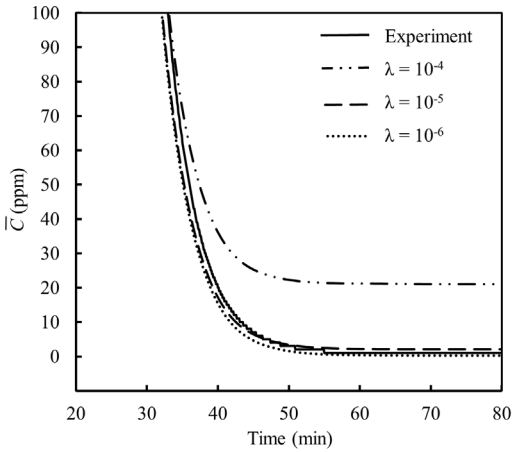

(b) Comparison between experiment and 0-D model.

Fig. 7. Effect of permeation factor in 2-D and 0-D models.

permeation), $\lambda = 10^{-5}$ (best fit), and $\lambda = 10^{-6}$ (lower permeation). Higher permeation leads to oxygen accumulation and overestimates residual oxygen levels, failing to match the experimental data. Lower permeation results in faster oxygen depletion, predicting near-zero levels faster than experimentally observed. The optimal match between simulated and experimental oxygen concentration curves is achieved at $\lambda = 10^{-5}$, validating this choice as the most appropriate approximation.

Comparisons Between Experimental and Numerical Analysis

Fig. 8 shows the average oxygen concentration over time for the experimental results, 2-D model and 0-D model, under different nitrogen flow rates. Across all flow rates, the 2-D and 0-D models exhibit trends similar to experimental results, demonstrating their predictive reliability. In practice, oxygen concentration should be decreased below 100 ppm. As a result, the required times to reach this concentration for each case are evaluated and listed in Table 2. It is noted that the required time is reduced with higher nitrogen flow rates due to faster flow velocities, which

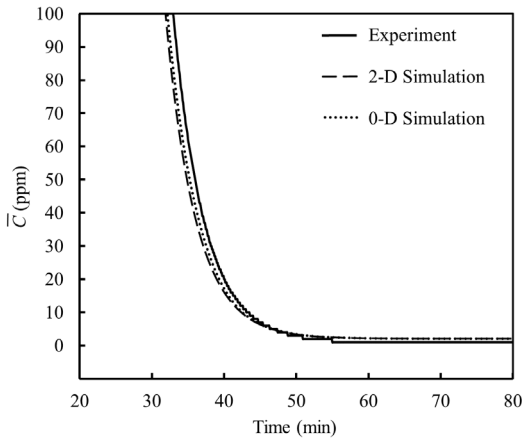

(a) $\dot{m}_{inN}$ =6.02×10^{-3} (kg/s).

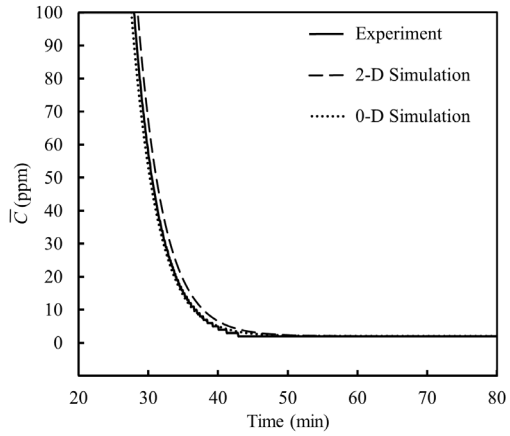

(b) $\dot{m}_{inN}$ =7.02×10^{-3} (kg/s).

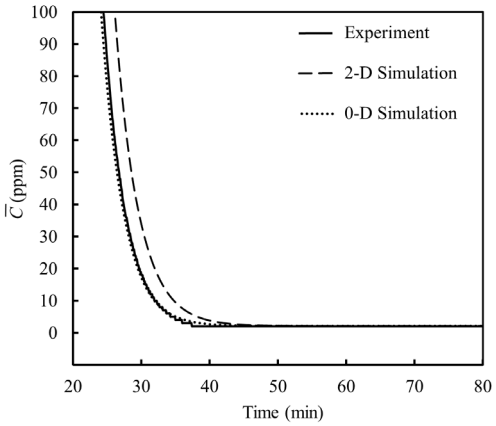

(c) $\dot{m}_{inN}$ =8.02×10^{-3} (kg/s).

Fig. 8. Comparison of average oxygen concentration variations under different nitrogen flow rates.

enhance the convective and diffusive mixing and expulsion of gases. The errors between the two models and experimental data are calculated to be within 3.3%, indicating that both models offer reliable predictions. Although the 2-D model introduces slightly higher errors due to simplified geometric representations, it still achieves satisfactory validation against

Table 1. Comparison of required time for experimental and numerical analysis.

$\dot{m}_{inN}$ (kg/s)	Time to reach 100 ppm (min.)			Error with experiment	
	Exp.	2-D	0-D	2-D	0-D
6.02×10^{-3}	33.00	31.91	32.16	-3.3%	-2.5%
7.02×10^{-3}	28.00	28.50	27.58	1.7%	-1.5%
8.02×10^{-3}	24.50	26.16	24.16	2.2%	-1.3%

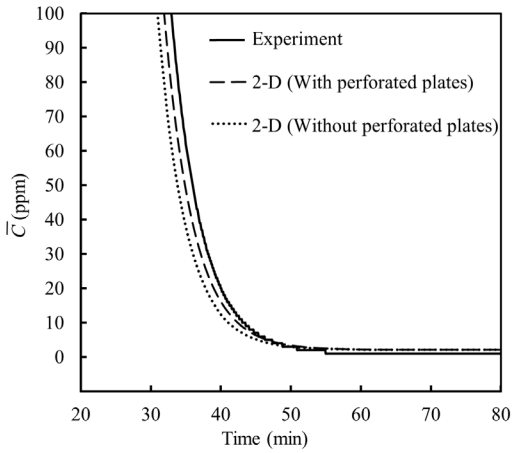

Fig. 9. Average oxygen concentration curve of the 2-D model with and without perforated plate.

experimental results. Both numerical models demonstrate strong agreement with experimental trends, showcasing their utility for predicting oxygen concentration dynamics in oxygen-free ovens with acceptable simulation error ranges.

Perforated plates are critical designs in an oxygen-free oven to enhance flow uniformity. Their effect on the average oxygen concentration in the 2-D model is shown in Fig. 9. In the case without perforated plates, the internal walls are removed. From the figure, the time to reach an average oxygen concentration of 100 ppm is 33.00 minutes with perforated plates, compared to 30.91 minutes without perforated plates, resulting in a time difference of 2.09 minutes. It is found that the 2-D model with perforated plates more accurately matches the experimental data. This result implies the importance of accurately modeling oven geometry, particularly flow paths influenced by perforated plates, to enhance the reliability of numerical simulations.

CONCLUSIONS

This study developed and validated two numerical models to analyze oxygen concentration variations in an oxygen-free oven: a two-dimensional model incorporating convection and diffusion effects and a zero-dimensional model focusing on mass conservation. The key findings are as follows:

1. The two-dimensional model accurately captured oxygen concentration distributions and flow characteristics, demonstrating that perforated plates improve uniformity and enhance gas flow stability, leading to better agreement with experimental data.
2. The zero-dimensional model presents an analytical expression of the time-dependent oxygen concentration, effectively predicting the concentration decreases over time.
3. Both models showed consistent trends with experimental measurements under different nitrogen flow rates, with deviations within 3.3%, confirming their predictive reliability.
4. The study highlighted the significance of air permeation effects, with simulations showing that a permeation factor of 10^{-5} yielded the best agreement with experimental data.
5. These findings provide a solid foundation for optimizing oxygen-free oven designs, offering insights into improved process control and system efficiency in industrial applications.

These results underscore the critical role of numerical modeling in enhancing the accuracy and efficiency of oxygen-free heat treatment processes. Future work may explore additional factors influencing oven performance, such as temperature variations and different gas compositions, to further refine predictive capabilities.

ACKNOWLEDGMENT

Financial support from the National Science and Technology Council, Taiwan, under Grant NSTC 112-2221-E-035-038-MY2, is greatly appreciated.

REFERENCES

Abraham, J. P., & Sparrow, E. M., "A Simple Model and Validating Experiments for Predicting the Heat Transfer to a Load Situated in an Electrically Heated Oven," *Journal of Food Engineering*, vol. 62, pp. 409-415, 2004.

Bejan, A., *Convection heat transfer*. John Wiley & Sons, 2013.

Isleroglu, H., & Kaymak-Ertekin, F., "Modelling of Heat and Mass Transfer during Cooking in Steam-Assisted Hybrid Oven," *Journal of Food Engineering*, vol. 181, pp. 50-58, 2016.

Kokolj, U., Škerget, L., & Ravnik, J., "A numerical model of the shortbread baking process in a forced convection oven, " *Applied Thermal Engineering*, vol. 111, pp. 1304-1311, 2017.

Lucchi, M., & Lorenzini, M., "Control-Oriented Low-Order Models for the Transient Analysis of a Domestic Electric Oven in Natural Convective Mode," *Applied Thermal Engineering*, vol. 147, pp. 438-449, 2019.

Maier, H. J., Herbst, S., Denkena, B., Dittrich, M.-A., Schaper, F., Worpenberg, S., Gustus, R., & Maus-Friedrichs, W., "Towards Dry Machining of Titanium-Based Alloys: A New Approach Using an Oxygen-Free Environment," *Metals*, vol. 10,1161, 2019.

Meinicke, S., Knipper, P., Helfenritter, C., & Wetzel, T., "A Lean Approach of Modeling the Transient Thermal Characteristics of Loop Heat Pipes Based on Experimental Investigations," *Applied Thermal Engineering*, vol. 147, pp. 895-907, 2018.

Meng, G.-H., Liu, H., Liu, M.-J., Xu, T., Yang, G.-J., Li, C.-X., & Li, C.-J., "Highly oxidation resistant MCrAlY bond coats prepared by heat treatment under low oxygen content," *Surface and Coatings Technology*, vol. 368, pp. 192-201, 2019.

Pei, Y., Jiang, S., Ding, Z., Cheng, L., Li, P., & Jiang, X., "Preparation and performance analysis of high-viscosity asphalt containing high-content SBS and crumb rubber by oxygen-free high-temperature treatment," *Construction and Building Materials*, vol. 402, pp. 132-763, 2023.

Ramirez-Laboreo, E., Sagues, C., & Llorente, S., "Dynamic Heat and Mass Transfer Model of an Electric Oven for Energy Analysis," *Applied Thermal Engineering*, vol. 93, pp. 683-691, 2016.

Strauß, C., Gustus, R., Maus-Friedrichs, W., Schöler, S., Holländer, U., & Möhwald, K., "Influence of atmosphere during vacuum heat treatment of stainless steels AISI 304 and 446," *Journal of Materials Processing Technology*, vol. 264, pp. 1-9, 2019.

Tan, C.-K., Jenkins, J., Ward, J., Broughton, J., & Heeley, A., "Zone Modelling of the Thermal Performances of a Large-Scale Bloom Reheating Furnace," *Applied Thermal Engineering*, vol. 50, pp. 1111-1118, 2013.

Tudon-Martinez, J. C., Cantu-Perez, A., Cardenas-Romero, A., & Lozoya-Santos, J. de J., "Mathematical Model-Based Design of an Industrial Box Furnace," *Applied Thermal Engineering*, vol. 161, pp. 114-153, 2019.

Verboven, P., Scheerlinck, N., De Baerdemaeker, J., & Nicolaï, B. M., "Computational Fluid Dynamics Modelling and Validation of the Temperature Distribution in a Forced Convection Oven," *Journal of Food Engineering*, vol. 43, pp. 61-73, 2000.

Wegewitz, L., Maus-Friedrichs, W., Gustus, R., Maier, H. J., & Herbst, S., "Oxygen-Free Production—From Vision to Application," *Advanced Engineering Materials*, vol. 25, 2201819, 2023.

Zhang, H., Chen, X., Xie, T., Yuan, B., Dai, H., He, S., & Liu, X., "Effects of reduced oxygen levels on flame propagation behaviors of starch dust deflagration," *Journal of Loss Prevention in the Process Industries*, vol. 54, pp. 146-152, 2018.

NOMENCLATURE

Variables

A_{in}	inlet area (m^2)
C	oxygen concentration (ppm)
$\bar{C}$	average oxygen concentration (ppm)
C_P	permeated oxygen concentration (ppm)
D	diffusion coefficient (m^2/s)
$\vec{F}$	volume force (N/m^3)
$\dot{m}_{inN}$	inlet mass flow rate of nitrogen (kg/s)
$\dot{m}_{inP}$	inlet mass flow rate of air permeation (kg/s)
$\dot{m}_{out}$	outlet mass flow rate (kg/s)
n	normal vector
p	pressure (Pa)
t	time (s)
$\vec{v}$	velocity vector (m/s)
$\forall$	volume of the oven (m^3)

Greek symbols

λ	permeation factor
μ	viscosity (Pa·s)
ρ	density (kg/m^3)
τ	tangent vector

Subscript

0	initial value